Molecular orbital structures in ^{10}Be

N. Itagaki[1,*] and S. Okabe[2]

[1]*Graduate School of Science, Hokkaido University, Sapporo 060-0810, Japan*
[2]*Center for Information and Multimedia Studies, Hokkaido University, Sapporo 060-0810, Japan*
(Received 7 April 1999; published 3 March 2000)

The structure of ^{10}Be is investigated using a microscopic $\alpha + \alpha + n + n$ model based on the molecular orbit (MO) model. The low-lying states are characterized by several configurations of valence neutrons, which are constructed as combinations of three basic orbits. The model space employed is extended from the traditional MO models, and the orbits are expressed as linear combinations of local Gaussians. Their positions are determined variationally. Using this model, we reanalyze the structure of ^{9}Be and show that this extension enables us to use the original two-body spin-orbit interaction determined from a scattering phase-shift analysis of α-n. In ^{10}Be, all of the observed positive-parity bands and the negative-parity bands are described within the model. The 0^+ ground state of ^{10}Be is described by a dominant $(3/2^-)^2$ configuration. The state has a rather large binding energy (8.38 MeV from the $\alpha + \alpha + n + n$ threshold experimentally), and the mechanism leading to binding, such as a pairing effect and reduction of the kinetic energy between two clusters, is discussed in detail. In spite of this large binding, the α-α clustering in the ground state persists due to a coupling effect between the ^{6}He$+\alpha$ configuration and the ^{5}He$+{}^5$He configuration, which provides a smooth potential for the valence neutrons. The second 0^+ state of ^{10}Be has a large α-α structure with a $(1/2^+)^2$ configuration. An enlargement of the α-α distance due to two-valence neutrons along the α-α axis makes their wave function smooth and reduces the kinetic energy drastically. Furthermore, the contribution of the spin-orbit interaction due to coupling between the $S_z=0$ and the $S_z=1$ configurations is important. We also show the mediation effect of two valence neutrons between two α clusters.

PACS number(s): 21.10.−k, 21.60.Gx

I. INTRODUCTION

Numerous experiments using unstable nuclear beams have succeeded in extending the observed neutron drip line, and various features of β-unstable nuclei have been revealed [1,2]. To discover new isotopes and exotic properties of weakly bound nuclei requires drastic changes in our understanding of the nuclear structure. For example, neutron halo structures in ^{6}He, ^{11}Li, ^{11}Be, ^{14}Be, ^{17}B, and ^{19}C suggest a breaking of the density saturation due to weakly bound neutrons [3]. Not only is the halo structure of weakly bound neutrons anomalous, but also the change of the shell structure. Experimental results show that the number of neutrons in the drip-line isotopes of p-shell nuclei Be and B go beyond the magic number $N=8$ (^{14}Be, $N=10$, and ^{19}B, $N=14$). In these nuclei, neutrons occupy orbits in higher shells (sd shell for Be). Since nuclei near the drip line are weakly bound systems, energy gaps between the shells become small. Recently, contributions of such higher shells were analyzed in $N=8$ nuclei. A calculation based on the shell model has shown that the slow β decay of ^{12}Be to ^{12}B can be explained by an admixture of the sd shell in ^{12}Be ($N=8$) in which the closed p-shell component must be less than 30% [4]. This shows that the concept of magic numbers is vague in ^{12}Be.

In the case of light nuclei, it has been shown that cluster structure appears in the vicinity of a threshold energy [5,6]. This model is an important candidate for explaining shell-structure anomalies. In the Be and B region, the α-α structure is well established, and especially in ^{9}Be, where a microscopic $\alpha + \alpha + n$ model has reproduced the properties of low-lying states [7,8]. In ^{10}Be, the microscopic α-cluster model has also been applied [9,10], and a developed cluster structure in the excited states was considered. According to this analysis of ^{9}Be, the α-α cluster structure of the core can reproduce not only natural parity states, but also the famous anomalous parity $1/2^+$ state at low energy [7,8]. It has been shown that the density of the $1/2^+$ state is polarized along the α-α axis, so that there is a strong mixing of the s-wave and the d-wave components. The ratio of the spectroscopic factors $S^{1/2^+}[s_{1/2}\times{}^8\text{Be}(0^+)]$ and $S^{1/2^+}[d_{5/2}\times{}^8\text{Be}(2^+)]$ is 0.79:0.30 [8]. This polarization of the neutron density due to the α-α core is an important mechanism to make the $1/2^+$ state low lying. This strong coupling feature of the $1/2^+$ state can be qualitatively interpreted in terms of deformed models as the [220] expression in the Nilsson diagram.

The intention of the present work is to analyze the structure of Be isotopes systematically beyond $N=8$ and to understand recent experimental data, including excited states based on the molecular orbit (MO) model. There have been pioneering studies for Be isotopes based on the MO model [9–11], where the properties of the low-lying states were qualitatively described, including the development of the α-α cluster structure in the excited states. However, to perform a systematic analysis of the structure of Be isotopes quantitatively over a wide energy range (~ 10 MeV), it is necessary to thoroughly improve the models. Here, we

*Present address: RI Beam Science Laboratory, RIKEN (The Institute of Physical and Chemical Research), Wako, Saitama, 351-0198, Japan. Electronic address: itagaki@postman.riken.go.jp

present a new framework in which the model space for valence neutrons is vastly extended. In the previous models, the valence neutrons have been treated as linear combinations of pure p orbits around each α cluster. We, however, solve the neutron motion around the α clusters and their wave functions are expressed by superpositions of Gaussians. Within this framework, the total wave function is fully antisymmetrized, and the angular momentum and parity are projected to good quantum numbers. The Coulomb interaction is included and the center-of-mass motion is correctly eliminated.

In this paper, we concentrate on a study of the ^{10}Be structure while emphasizing a structure analysis of the ground and second 0^+ states. The study starts with a reanalysis of ^{9}Be to examine the effective interactions, especially the spin-orbit interaction. Since the spin-orbit interaction acts repulsively for the neutron, which occupies the $1/2^-$ orbit, the neutron in $1/2^-$ has a more extended density distribution than $3/2^-$. We use the MO model space scaled up largely in comparison with previous MO model studies [9,10]; it will be shown that this difference of the density distribution is taken into account within the present framework. This enables us to use the original spin-orbit interaction determined by a phase-shift analysis. Both the positive- and negative-parity bands are described as combinations of three basic orbits introduced in ^{9}Be ($3/2^-$, $1/2^+$, and $1/2^-$). The α-α structure in the ground 0^+ state persists where two valence neutrons occupy mainly the $3/2^-$ orbit. The binding mechanism (8.5 MeV from the $\alpha+\alpha+n+n$ threshold, especially the pairing and kinetic energy effects) will be discussed. The second 0^+ state has a larger α-α distance where two valence neutrons occupy mainly the $1/2^+$ orbit. A candidate for the 4^+ state of this band with large α-α clustering has been recently observed [12], and our results will be compared with the experimental data.

This paper is organized as follows. In Sec. II, we give a description of the single-particle orbits around the two α clusters whose model space is vastly extended from the traditional MO models. In Sec. III, we reanalyze ^{9}Be and discuss especially the spin-orbit interaction. In Sec. IV, the construction of the basis states for ^{10}Be is explained. In Sec. V, the level structure of ^{10}Be is presented, and the large α-α distance due to the valence neutrons is studied in the second 0^+ state. The binding mechanisms for the ground and the second 0^+ states are discussed in Sec. VI, and the conclusion is given in Sec. VII.

II. FRAMEWORK

A microscopic $\alpha+\alpha+n+n$ cluster model is introduced for ^{10}Be in order to clarify the relation between the configurations of the valence neutrons and the α-α distance. The configurations for the valence neutrons are introduced based on the MO picture [11]. The MO model has been applied for a structural analysis of Be isotopes [9,10], and the results have proved that the basic ideas of the MO model work well, especially for ^{9}Be and ^{10}Be. Namely, the valence neutrons are considered to occupy orbits around both α clusters. In ^{9}Be, the calculated energy surface and the density distribution for a valence neutron have supported this picture.

Within the present framework, the MO model is used to classify the single-particle orbit, and the model space is extended from the traditional version applied so far to Be isotopes. Now, the total wave function is fully antisymmetrized and expressed by a superposition of terms centered at different relative distances between the two α clusters (d) with various configurations of two valence neutrons ($c1$ and $c2$). Here, χ represents the spin-isospin ($p\uparrow$, $p\downarrow$, $n\uparrow$ and $n\downarrow$) function:

$$\Psi_M^J = \sum_{d,c1,c2,K} f_{c1,c2}^{d,K} P_{MK}^J \Phi_{c1,c2}^d, \tag{1}$$

$$P_{MK}^J = \frac{2J+1}{8\pi^2} \int d\Omega D_{MK}^{J*}(\Omega)\hat{R}(\Omega), \tag{2}$$

$$\Phi_{c1,c2}^d = \mathcal{A}[\phi_1^{(\alpha)}\phi_2^{(\alpha)}(\phi_{c1}\chi_{c1})(\phi_{c2}\chi_{c2})]. \tag{3}$$

The projection to the eigenstates of angular momentum J is performed numerically, where Ω is the Euler angle. The diagonalization of the Hamiltonian is carried out and $\{f_{c1,c2}^{d,K}\}$ are obtained after the projection. All nucleons are described by Gaussians with the oscillator parameter s equal to 1.46 fm. The α clusters located at $d/2$ and $-d/2$ on the z axis contain four nucleons:

$$\phi^{(\alpha)} = G_{R_\alpha}^{p\uparrow}G_{R_\alpha}^{p\downarrow}G_{R_\alpha}^{n\uparrow}G_{R_\alpha}^{n\downarrow}\chi_{p\uparrow}\chi_{p\downarrow}\chi_{n\uparrow}\chi_{n\downarrow}. \tag{4}$$

G represents Gaussians:

$$G_{R_\alpha} = \left(\frac{2\nu}{\pi}\right)^{3/4}\exp[-\nu(\vec{r}-\vec{R}_\alpha)^2], \quad \nu = 1/2s^2,$$

$$\vec{R}_\alpha = \{d\vec{e}_z/2, \quad -d\vec{e}_z/2\}. \tag{5}$$

The configurations for the valence neutrons ($\phi_{c1}\chi_{c1}$ and $\phi_{c2}\chi_{c2}$) are expressed by a linear combination of local Gaussians:

$$\phi_{ci}\chi_{ci} = \sum_j g_j G_{R_n^j}\chi_{ci}, \quad i = 1,2, \tag{6}$$

$$G_{R_n^j} = \left(\frac{2\nu}{\pi}\right)^{3/4}\exp[-\nu(\vec{r}-\vec{R}_n^j)^2], \quad \nu = 1/2s^2. \tag{7}$$

In the MO model, the valence neutrons are expressed by a linear combination of orbits around two α clusters. An orbit around each α cluster is called an atomic orbit (AO). Here, we must notice that the valence neutrons and neutrons in the α clusters are identical particles, and antisymmetrization imposes the AO forbidden space. The lowest AO has one node and parity minus, that is, the p orbit. When a linear combination of two AOs (p orbit) around the left α cluster and the right α cluster is summed up by the same sign, the resultant MO also has negative parity and one node. In this case, the MO is restricted to spread along an axis perpendicular to the α-α (z) axis, that is, the so-called π orbit. It cannot spread along the z axis where the two α clusters are already located.

(a) π-orbit   One node

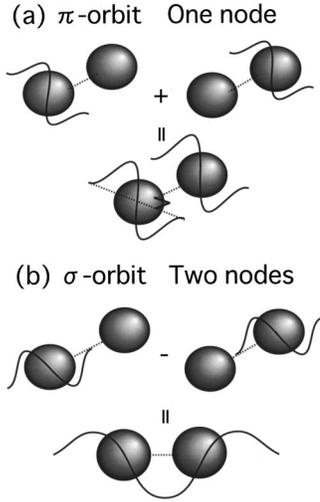## (b) σ-orbit   Two nodes

FIG. 1. Schematic figure for a single valence neutron: (a) π orbit and (b) σ orbit.

If two p orbits are summed up by different signs, the resultant MO has two nodes and positive parity. This MO can spread to all directions, and the optimal direction becomes the z direction. This is the so-called σ orbit, and the energy becomes lower as the distance between two α clusters increases.

Each valence neutron is introduced to have a definite K^π at the zero limit of centers of the local Gaussians ($\{R_n^j\}$), but the precise position of $\{R_n^j\}$ is determined variationally for each α-α distance before the angular momentum projection. When we determine the final level structure after the angular momentum projection, the coefficients $\{g_j\}$ are treated as variational parameters to take into account deviations from the original orbits. Three basic orbits are introduced for the Be isotopes, $\bar{K}=3/2^-$, $1/2^-$, and $1/2^+$, where $\bar{K}$ corresponds to the z component of the angular momentum (K) at the zero limit of the centers of local Gaussians ($\{R_n^j\}$). The $1/2^+$ state is the σ orbit, and the spin-orbit interaction splits the π orbit to $3/2^-$ and $1/2^-$. We call the π orbit a ''ring orbit'' because it spreads perpendicular to the α-α axis and rotates around it. We call the σ orbit a ''chain orbit'' spreading along the α-α axis, which is a higher-nodal orbit weakly moving around two α clusters. Schematic figures for these orbits are drawn in Fig. 1.

The main difference between this framework and the traditional MO model [9,10] is the treatment of the orbits around the α clusters. In the traditional MO model, the AO around the α cluster has been expressed by the jj-coupling scheme. The valence neutrons for the $3/2^-$ state and those for the $1/2^-$ state have been introduced to have the same radial distribution; thus, the strength of the spin-orbit interaction has been weakened to less than half to reproduce the ls splitting. However, we extend the model space by expressing the p orbit around the α cluster as a combination of two local Gaussians; their rotation radii are dependent on the orbits. Therefore, now we can use the original spin-orbit interaction derived from the phase-shift analysis on the $\alpha+n$ scattering.

In ^{10}Be, since two valence neutrons occupy these single-particle orbits, three configurations with the total $\bar{K}=\bar{K}_1+\bar{K}_2=0$ are generated. For the ground-state configuration, each valence neutron has only one node, and the direction of the orbit is restricted to be perpendicular to the α-α (z) axis. This is a π orbit. The π orbit is constructed as a linear combination of p_x and p_y orbits. They are expressed as two Gaussians whose centers are shifted by a variational parameter b,

$$p_x = G_{+b\vec{e}_x} - G_{-b\vec{e}_x}, \quad p_y = G_{+b\vec{e}_y} - G_{-b\vec{e}_y}. \quad (8)$$

For the ground state, the spatial part and the spin part of $\bar{K}$ are introduced to be parallel so that the spin-orbit interaction acts attractively. Then, K^π of the two valence neutrons are $\bar{K}_1^\pi = 3/2^-$ and $\bar{K}_2^\pi = -3/2^-$, and

$$\Phi(3/2^-, -3/2^-) = \mathcal{A}[\phi_1^{(\alpha)}\phi_2^{(\alpha)}(\phi_{c1}\chi_{c1})(\phi_{c2}\chi_{c2})]. \quad (9)$$

The spin-up valence neutron ($|n\uparrow\rangle$) has $\bar{K}_1^\pi = 3/2^-$ (rY_{11}) and the spin-down valence neutron ($|n\downarrow\rangle$) has $\bar{K}_1^\pi = 3/2^-$ (rY_{1-1}), which are expressed as linear combinations of p_x and p_y. The MO consists of two AOs around the α clusters. Then, we introduce the variational parameter a, a distance along the z axis, and describe the MO as a combination of p orbits centered at $+a$ and $-a$ [denoted as $(AO)_{+a}$, $(AO)_{-a}$]. Thus, the valence neutrons for the ground state are described as follows:

$$\phi_{c1}\chi_{c1} = \{(p_x + ip_y)_{+a} + (p_x + ip_y)_{-a}\}|n\uparrow\rangle, \quad (10)$$

$$\phi_{c2}\chi_{c2} = \{(p_x - ip_y)_{+a} + (p_x - ip_y)_{-a}\}|n\downarrow\rangle. \quad (11)$$

Here,

$$(p_x)_{+a} = G_{a\vec{e}_z + b\vec{e}_x} - G_{a\vec{e}_z - b\vec{e}_x},$$

$$(p_y)_{+a} = G_{a\vec{e}_z + b\vec{e}_y} - G_{a\vec{e}_z - b\vec{e}_y}. \quad (12)$$

The orbit $(p_x)_{+a} = \exp\{-\nu[\vec{r} - (a\vec{e}_z + b\vec{e}_x)]^2\} - \exp\{-\nu[\vec{r} - (a\vec{e}_z - b\vec{e}_x)]^2\}$ is illustrated by using a and b in Fig. 2(a). These free parameters a and b are optimized for each value of the α-α distance.

We also define a basis state in which the spin-orbit interaction acts repulsively. The spatial part and the spin part of the momenta, $\bar{K}$, are antiparallel, $\bar{K}_1^\pi = 1/2^-$, $\bar{K}_2^\pi = -1/2^-$:

$$\Phi(1/2^-, -1/2^-) = \mathcal{A}[\phi_1^{(\alpha)}\phi_2^{(\alpha)}(\phi_{c1}\chi_{c1})(\phi_{c2}\chi_{c2})], \quad (13)$$

$$\phi_{c1}\chi_{c1} = \{(p_x + ip_y)_{+a} + (p_x + ip_y)_{-a}\}|n\downarrow\rangle, \quad (14)$$

$$\phi_{c2}\chi_{c2} = \{(p_x - ip_y)_{+a} + (p_x - ip_y)_{-a}\}|n\uparrow\rangle. \quad (15)$$

Furthermore, we prepare a chain orbit expressed by subtracting two AOs at $+a = d/2$ and $-a = -d/2$:

$$\Phi(1/2^+, -1/2^+) = \mathcal{A}[\phi_1^{(\alpha)}\phi_2^{(\alpha)}(\phi_{c1}\chi_{c1})(\phi_{c2}\chi_{c2})], \quad (16)$$
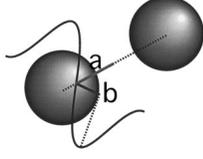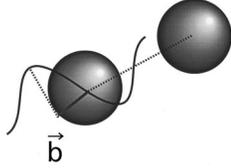
(a) $(P_x)_{+a}$ for the π-orbit

(b) $(\vec{P})_a$ for the σ-orbit

FIG. 2. Variational parameters describing a valence neutron: (a) $(p_x)^a$ for the π orbit and (b) $\vec{p}^b$ for the σ orbit.

$$\phi_{c1}\chi_{c1}=\{(\vec{p})_{+a}-(\vec{p})_{-a}\}|n\uparrow\rangle, \quad a=d/2, \quad (17)$$

$$\phi_{c2}\chi_{c2}=\{(\vec{p})_{+a}-(\vec{p})_{-a}\}|n\downarrow\rangle, \quad a=d/2. \quad (18)$$

Since the σ orbit has two nodes, it can spread in all directions; the direction is determined variationally. In this case, we impose no restrictions on the direction of the AO:

$$(\vec{p})_{\pm a}=(G_{+\vec{b}}-G_{-\vec{b}})_{\pm a}. \quad (19)$$

An orbit $(\vec{p})_{+a}=\exp\{-\nu[\vec{r}-(a\vec{e}_z+\vec{b})]^2\}-\exp\{-\nu[\vec{r}-(a\vec{e}_z-\vec{b})]^2\}$ is illustrated by using $\vec{b}$ in Fig. 2(b). As a result of a variational calculation, the direction of $\vec{b}$ is optimized along the z-axis ($\bar{K}_1^\pi=1/2^+$, $\bar{K}_2^\pi=-1/2^+$).

The spin-triplet basis states are also prepared. For a ring orbit (π orbit), $\Phi(3/2^-,-1/2^-)$, $\bar{K}^\pi=1^+$ is constructed from $\bar{K}_1^\pi=3/2^-$ and $\bar{K}_2^\pi=-1/2^-$ ($S_z=1$). In the case of a chain orbit (σ orbit), the two spin-up valence neutrons cannot occupy the same $\bar{K}^\pi=1/2^+$ due to the Pauli principle. As a result of a variational calculation, the spin-triplet chain orbit (σ orbit) is found to deviate from the z axis, and has a small component along the x direction.

The negative-parity states of ^{10}Be are prepared as follows: one valence neutron occupies a ring orbit (π orbit) with negative parity and another occupies a chain orbit (σ orbit) with positive parity. In this way configurations with z components of the spin $S_z=0$ and $S_z=1$ can be constructed. The $S_z=0$ configuration is constructed as $\Phi(3/2^-,-1/2^+)$ with the total $\bar{K}^\pi=1^-$:

$$\Phi(3/2^-,-1/2^+)=\mathcal{A}[\phi_1^{(\alpha)}\phi_2^{(\alpha)}(\phi_{c1}\chi_{c1})(\phi_{c2}\chi_{c2})], \quad (20)$$

$$\phi_{c1}\chi_{c1}=\{(p_x+ip_y)_{+a}+(p_x+ip_y)_{-a}\}|n\uparrow\rangle, \quad (21)$$

$$\phi_{c2}\chi_{c2}=\{(p)_{+a}-(p)_{-a}\}|n\downarrow\rangle \quad a=d/2. \quad (22)$$

The $S_z=1$ configuration is constructed as $\Phi(3/2^-,1/2^+)$ with the total $\bar{K}^\pi=2^-$:

$$\Phi(3/2^-,1/2^+)=\mathcal{A}[\phi_1^{(\alpha)}\phi_2^{(\alpha)}(\phi_{c1}\chi_{c1})(\phi_{c2}\chi_{c2})], \quad (23)$$

$$\phi_{c1}\chi_{c1}=\{(p_x+ip_y)_{+a}+(p_x+ip_y)_{-a}\}|n\uparrow\rangle, \quad (24)$$

$$\phi_{c2}\chi_{c2}=\{(p)_{+a}-(p)_{-a}\}|n\uparrow\rangle \quad a=d/2. \quad (25)$$

To include all combinations of the ring orbits and chain orbits among the basis states for negative parity, we construct bases of $\bar{K}_1^\pi=1/2^-$ and $\bar{K}_2^\pi=1/2^+$; $\Phi(-1/2^-,-1/2^+)$ has $\{S_z=0,\bar{K}^\pi=-1^-\}$, and $\Phi(-1/2^-,1/2^+)$ has $\{S_z=1,\bar{K}^\pi=0^-\}$. The contributions of these states give only small corrections; nevertheless, we do include them in the basis of the negative-parity states.

III. REANALYSIS OF ^{9}Be

The Hamiltonian has the following form:

$$\mathcal{H}=\sum_i T_i-T_{c.m.}+\sum_{i<j}V_{ij}+\sum_{i<j}V_{ij}^{ls}$$

$$+\sum_{i<j}\frac{e^2}{4r_{ij}}(1-\tau_z^i)(1-\tau_z^j). \quad (26)$$

As effective nucleon-nucleon interactions, we use Volkov No. 2 [13] for the central part with the Majorana exchange parameter $M=0.6$ ($W=0.4$), the Bartlett exchange parameter $B=0.125$, and the Heisenberg exchange parameter $H=0.125$ (using B and H, there is no neutron-neutron bound state):

$$V_{ij}=\{V_1e^{-a_1r_{ij}^2}-V_2e^{-a_2r_{ij}^2}\}\{W-MP^\sigma P^\tau+BP^\sigma-HP^\tau\}, \quad (27)$$

where $V_1=-60.650$ MeV, $V_2=61.140$ MeV, $a_1=0.980$ fm^{-2}, and $a_2=0.309$ fm^{-2}. For the spin-orbit part, we use the G3RS spin-orbit term [14], which is a two-range Gaussian with a projection operator onto the triplet odd state (P_{31}),

$$V_{ij}^{ls}=V_0^{ls}\{e^{-a_1r_{ij}^2}-e^{-a_2r_{ij}^2}\}\vec{L}\cdot\vec{S}P_{31}. \quad (28)$$

The strength parameter is $V_0^{ls}=2000$ MeV, $a_1=5.00$ fm^{-2}, and $a_2=2.778$ fm^{-2}. All of these parameters are determined from the $\alpha+n$ and $\alpha+\alpha$ scattering phase shifts and the binding energy of the deuteron [8].

These parameters are the same as those used in the fully microscopic $\alpha+\alpha+n$ model for ^{9}Be [8]. However, in the analyses for Be isotopes based on the MO model [9], the strength of the spin-orbit interaction (V_0^{ls}) has been weakened to less than half (900 MeV), since the model space of valence neutrons has been truncated to a pure p orbit around each α cluster.

We summarize the relation between the model space and the spin-orbit strength discussed in the previous paper, Ref. [8]. Figure 3 shows the energy curve for the $3/2^-$ state and
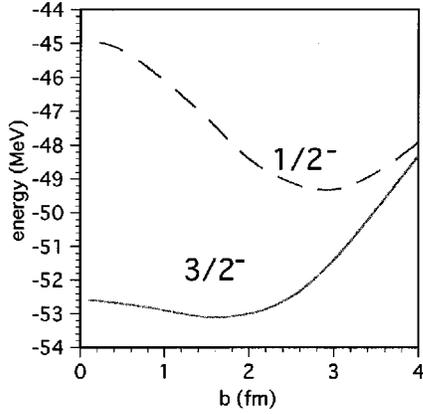
FIG. 3. The energies of the $3/2^-$ state and the $1/2^-$ state as a function of parameter b in ^{9}Be. $d=2a=3.5$ fm.

that for the $1/2^-$ state using the original V_0^{ls} (2000 MeV). The abscissa expresses the position of the Gaussian center on the x axis for a valence neutron measured from the center of the α cluster (parameter b). Since the repulsive contribution of the spin-orbit interaction for the $1/2^-$ state is strong near the α cluster, a minimal energy of $1/2^-$ is seen around $b=3$ fm, which is much longer than that for $3/2^-$.

The truncated model space in the traditional MO model corresponds to the limit of $b=0$, and the energy difference between these two states here is much larger than the energy difference between states with optimal b values. As listed in Table I, the spin-orbit splitting has been calculated to be 7.9 MeV compared with the experimental value of 2.8 MeV. (The model space in the traditional MO model is realized by employing $a=d/2$ and $b=0.1$ fm.) With the use of $V_0^{ls}=900$ MeV, the splitting is reduced to 3.6 MeV; this is the reason why the strength is artificially weakened in the traditional MO model.

In the present model space, the value of b in the $1/2^-$ state, in which the spin-orbit interaction acts repulsively, is allowed to be larger than that for the $3/2^-$ state. The valence neutron escapes from the core to reduce the matrix element of the spin-orbit interaction. As shown in Table I, the energy splitting between these states is obtained to be 4.0 MeV with the use of the original spin-orbit interaction ($V_0^{ls}=2000$ MeV). As a result, the ratio of the contributions of the spin-orbit interaction for the two states is very different from the ratio of $-1:2$ expected from a simple shell model. The spin-orbit components in $3/2^-$ and $1/2^-$ were calculated to be -3.1 MeV and 1.1 MeV in ^{9}Be. This change of ratio from the simple shell model is one of the characteristic properties of a weakly bound (or unbound) system.

One may think that a splitting of 4.0 MeV is still larger than the experimental splitting of 2.8 MeV. However, this is a rather good approximation, since in ^{9}Be, this problem is never overcome without solving the tail of the valence neutron carefully. The splitting reflects not only the spin-orbit interaction, but also the kinetic energy. In the brackets of Table I, the kinetic energies of the $3/2^-$ and $1/2^-$ states are listed for three model spaces: (I) a and b are fixed to $a=d/2$, $b=0.1$ fm (model space in the traditional MO model); (II) a and b are freely changed (present model space); (III) a and b are regarded as generator coordinates. In the last case, wave functions with different a,b values are superposed, and the tail of a neutron is correct. The reduction of the kinetic energy from the present model space (II) to the generator coordinate model space (III) is 3.8 MeV (112.5 MeV $\rightarrow$108.7 MeV) for the $1/2^-$ which is much larger than 2.3 MeV for the $3/2^-$ state (119.4 MeV$\rightarrow$117.1 MeV). Therefore, an accurate description of the tail enables a reduction of the splitting of these states to 3.2 MeV ($3/2^-$ -56.1 MeV, $1/2^-$ -52.9 MeV).

Through these analyses, it becomes clear that the interaction determined from a phase-shift analysis of α-α and α-n can reproduce the properties of ^{9}Be due to the extension of the model space; we then analyze the ^{10}Be nucleus using the same interaction.

IV. CONSTRUCTION OF THE BASIS STATES

In ^{10}Be, we adopt three 0^+ configurations $[(3/2^-)^2,(1/2^-)^2,(1/2^+)^2]$, since three single-particle orbits ($\bar{K}=3/2^-,1/2^-,1/2^+$) have been introduced. The values of the parameters for the valence neutrons are obtained variationally. As shown in Fig. 2, parameter a describes the z component of the position of the Gaussian center, and parameter b corresponds to the rotation radius of the π orbit around the α-α core. The parameter $\vec{b}$ corresponds to the rotation radius for the case of the σ orbit. These values are optimized by using the cooling method used in the antisymmetrized molecular dynamics (AMD) [15–19] developed by En'yo and co-workers for each α-α distance before the angular momentum projection. The obtained values of these parameters are listed in Table II along with the energies for the cases of $\Phi(3/2^-,-3/2^-)$ (upper panel), $\Phi(1/2^-,-1/2^-)$ (lower panel) for α-α distances of 2–5 fm.

For $\Phi(3/2^-,-3/2^-)$, $d=2$ fm gives the minimal intrinsic energy (-52.09 MeV). After an angular momentum projection, the 0^+ state has an energy minimum at $d=3$ fm (the 0^+ state -58.01 MeV). The optimal distance is longer than

TABLE I. The energies of ^{9}Be for the model space of the traditional MO model (left) where a and b are fixed to $a=d/2$, $b=0.1$ fm (I). (II) The energies for the present model space (middle) where a and b are chosen freely. (III) The energies for a model space which is spanned by a and b being generator coordinates (right). The values in parentheses are the kinetic energies. The unit is MeV.

J^π	(I) $a=d/2$, $b=0.1$ fm	(II) a,b free	(III) a,b generator coordinates
$1/2^-$	-46.2 (123.4)	-50.8 (112.5)	-52.9 (108.7)
$3/2^-$	-54.1 (125.8)	-54.8 (119.4)	-56.1 (117.1)

TABLE II. The values of a, b, and the intrinsic energy and the 0^+ energy as a function of the α-α distance. The wave function of ^{10}Be is $\Phi(3/2^-, -3/2^-)$ (upper panel), $\Phi(1/2^-, -1/2^-)$ (lower panel).

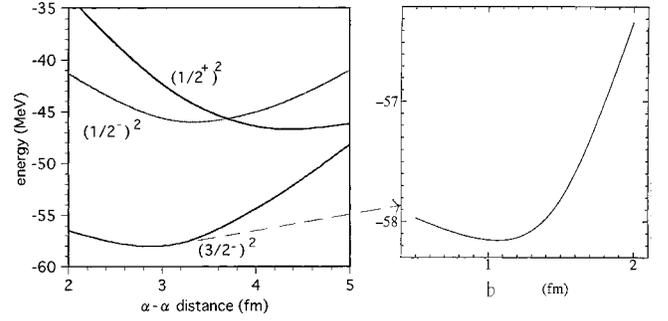| α-α (fm)	a (fm)	b (fm)	Intrinsic (MeV)	0^+ (MeV)
2	1.09	0.99	-52.09	-56.51
3	1.39	1.08	-50.91	-58.01
4	1.71	1.35	-44.64	-54.40
5	2.12	1.53	-38.04	-48.16
α-α (fm)	a (fm)	b (fm)	Intrinsic (MeV)	0^+ (MeV)
2	1.33	2.05	-38.06	-41.32
3	1.49	2.11	-39.30	-45.62
4	1.63	2.21	-35.42	-45.03
5	1.89	2.35	-30.34	-41.01

FIG. 4. The 0^+ energy curve for $\Phi(3/2^-, -3/2^-)$, $\Phi(1/2^-, -1/2^-)$, and $\Phi(1/2^+, -1/2^+)$ as a function of the α-α distance (d) (left panel). The 0^+ energy curve for $\Phi(3/2^-, -3/2^-)$ as a function of b, the distance of the valence neutrons from the α particles (right panel). The α-α distance is 3 fm. The minimal energy is found at $b=1.1$ fm, which coincides with the optimal value of b before the angular momentum projection.

that for the intrinsic energy. Here, the parameter $+a$ (z component of the position of the Gaussian center) is obtained to be approximately the same value as $d/2$. Therefore, the picture ''AO around the α cluster'' works well even if we allow a deviation of the AO along the z axis. As shown in Table II, $a=1.39$ fm for $d=3$ fm, and the deviation from $d/2$ is only 0.11 fm. For $d=5$ fm, $a=2.12$ fm, and it is smaller than $d/2$ by 0.38 fm. When the α-α distance becomes large, the valence neutrons shift a little inside to gain potential energy.

The parameter b (rotation radius around the α cluster) depends on the configurations. For $\Phi(3/2^-, -3/2^-)$, b is obtained to be approximately 1 fm, but for $\Phi(1/2^-, -1/2^-)$, the rotation radius becomes longer, by about 2 fm, since the spin-orbit interaction acts attractively for $\Phi(3/2^-, -3/2^-)$ and repulsively for $\Phi(1/2^-, -1/2^-)$. Therefore, the orbits around the α clusters should be expressed for the configurations one by one to estimate the spin-orbit splitting correctly. This is the reason why we express the AO as a linear combination of the local Gaussians. In the traditional MO model, the AO has been the eigenstate of the angular momentum around the α clusters with a common oscillator parameter. This corresponds to the limit of $a=d/2$ and $b=0$ in our model. Now, the optimal value of b for the neutron in the $3/2^-$ state in ^{10}Be (2 fm) is smaller than that in ^{9}Be (3 fm), and distribution of the neutron in ^{10}Be is more compact.

We now construct a basis state for the second 0^+ state. Table III gives the results for $\Phi(1/2^+, -1/2^+)$. It is signifi-

TABLE III. Values of a, $\vec{b}$, and the intrinsic energy and the 0^+ energy as a function of the α-α distance. The wave function is $\Phi(1/2^+, -1/2^+)$.

α-α (fm)	b_x (fm)	b_y (fm)	b_z (fm)	Intrinsic (MeV)	0^+ (MeV)
2	0.00	0.00	1.93	-32.83	-33.87
3	0.00	0.00	2.04	-38.57	-42.28
4	0.00	0.00	2.02	-39.96	-46.39
5	0.00	0.00	1.56	-38.20	-46.16

cant to point out that $\vec{b}$ has only the z component. Thus, the four-body system ($\alpha + \alpha + n + n$) has a linear configuration. Moreover, the α-α distance which minimizes the 0^+ energy is between 4 fm (-46.54 MeV) and 5 fm (-46.38 MeV), 1 fm longer than $\Phi(3/2^-, -3/2^-)$. The valence neutrons along the α-α axis enhance the α-α distance and weakly couple the α clusters. The 0^+ state energy of $\Phi(1/2^+, -1/2^+)$ is lower than that of $\Phi(1/2^-, -1/2^-)$. Therefore, the level inversion of $1/2^+$ and $1/2^-$ in ^{9}Be and ^{11}Be is also reflected in ^{10}Be.

Now, at an α-α distance (d) of 4 fm, the 0^+ energy of $\Phi(1/2^+, -1/2^+)$ is equal to -46.54 MeV using the optimized rotation radius for neutrons ($|\vec{b}|=2.02$ fm). When we take the zero limit for $|\vec{b}|$ to be the same as in the traditional MO model, this energy becomes -44.39 MeV, which is higher by more than 2 MeV. Therefore, the effect of making the value of b (rotation radius) a free parameter is very important for the σ orbit. Since the σ orbit is a higher nodal orbit, this smoothness of the wave function reduces the kinetic energy significantly.

The 0^+ energy curves for $\Phi(3/2^-, -3/2^-)$, $\Phi(1/2^-, -1/2^-)$, and $\Phi(1/2^+, -1/2^+)$ are summarized in the left hand panel of Fig. 4. The energy of $\Phi(1/2^+, -1/2^+)$ becomes lower as d increases, and the minimal energy is lower than that of $\Phi(1/2^-, -1/2^-)$ (level inversion). Here, the energy difference between $\Phi(1/2^+, -1/2^+)$ and $\Phi(1/2^-, -1/2^-)$ is small; later, though, it will be shown that coupling with $\Phi(3/2^-, -3/2^-)$ pushes up the third 0^+ dominated by $\Phi(1/2^-, -1/2^-)$, and coupling with the spin-triplet basis state dominated by $\Phi(1/2^+, -1/2^+)$ makes the second 0^+ lower. Therefore, this level inversion is finally much enhanced.

These parameter optimizations have been performed before the angular momentum projection. Although this is an approximation, we show that the parameters obtained are close to the one which minimizes the energy after the angular momentum projection. This agreement comes from the K^π projection for each valence neutron, which is expressed by a linear combination of Gaussians in this framework. The

TABLE IV. Values of a, b for one valence neutron and $\vec{b}$ for another valence neutron, the intrinsic energy, the $1^-(K=1)$ (upper panel), and the $2^-(K=2)$ (lower panel) energy as a function of the α-α distance. The wave functions of ^{10}Be are $S_z=0\Phi(3/2^-,-1/2^+)$ (upper panel) and $S_z=1\Phi(3/2^-,1/2^+)$ (lower panel).

α-α (fm)	a (fm)	b (fm)	b_x (fm)	b_y (fm)	b_z (fm)	Intrinsic (MeV)	$1^-(K=1)$ (MeV)
2	1.20	0.96	0.18	0.00	1.83	−40.22	−41.29
3	1.43	1.08	0.04	0.00	1.95	−42.97	−46.76
4	1.74	1.30	0.19	0.00	1.92	−40.83	−47.67
5	2.11	1.50	0.35	0.00	1.80	−36.63	−45.12

α-α (fm)	a (fm)	b (fm)	b_x (fm)	b_y (fm)	b_z (fm)	Intrinsic (MeV)	$2^-(K=2)$ (MeV)
2	1.18	1.00	0.15	0.00	1.90	−39.09	−39.70
3	1.43	1.15	0.16	0.00	2.03	−41.79	−45.51
4	1.76	1.41	0.13	0.00	2.16	−39.59	−46.30
5	2.17	1.50	0.11	0.00	1.79	−35.30	−43.57

0^+ energy curve for $\Phi(3/2^-,-3/2^-)$ with respect to b (the distance of valence neutrons from the α cluster) is shown in the right hand panel of Fig. 4, where parameters a and d are fixed to $2a=d=3.0$ fm. The 0^+ energy minimum (-58.2 MeV) is seen around $b=1.1$ fm. This value is almost the same as 1.08 fm in Table II obtained before the angular momentum projection. Therefore, the value of the optimized b does not depend on the projection of the total angular momentum during the optimization if the K^π of each valence neutron is projected. Without the K^π projection for each neutron, the value of b (the rotation radius for valence neutrons around a core nucleus) would become too small to eliminate higher-nodal waves around the α-α axis, such as the s wave and d wave.

The negative-parity states $\Phi(3/2^-,-1/2^+)$ and $\Phi(3/2^-,1/2^+)$ are listed in Table IV. Since one valence neutron is a chain orbit, the large α-α distance also gives rise to the appearance of low-lying negative-parity states. Both $K^\pi=1^-$ and $K^\pi=2^-$ have their minimum at around the α-α distance of 4 fm. Their energies are very close, and mixing of the two bands is expected to have a large effect on the 2^- state.

V. RESULTS

In this section, we present the results for ^{10}Be. First, we show the level structure. There appear both the ground state and the second 0^+ rotational band. Next, the coupling effects between the basis states introduced are shown, and the enlargement of the α-α distance in the second 0^+ state due to the $(1/2^+)^2$ configuration will be clarified.

A. Energy level

The basis states obtained above are combined using the generator coordinate method (GCM). The basis states employed are listed in Table V, and the energy levels of ^{10}Be are calculated in the bound-state approximation, with the result shown in Fig. 5.

Three 0^+ states appear. Their dominant valence neutron components are $(3/2^-)^2$ for the ground state, $(1/2^+)^2$ for the second 0^+ state, and $(1/2^-)^2$ for the third 0^+ state. The total energy of the ground state is calculated to be -61.4 MeV, which corresponds to -7.3 MeV with respect to the $\alpha+\alpha+n+n$ threshold (the experimental value is -8.4 MeV). The 0_2^+ state and the 0_3^+ state are obtained at excitation energies of 8.1 MeV and 11.6 MeV, respectively. From the ground and the second 0^+ states, the $K^\pi=0$ rotational bands are formed as (i) 0_1^+ (0.0 MeV) -2_2^+ (3.3 MeV) -4_1^+ (10.7 MeV) and (ii) 0_2^+ (8.1 MeV) -2_3^+ (9.5 MeV) -4_2^+ (12.5 MeV). The level spacing of 0_1^+ -2_1^+ is 3.3 MeV, which corresponds nicely to the experimental value in ^{10}Be (3.37 MeV), which is almost comparable with the case of ^{8}Be (~3 MeV). On the contrary, the second 0^+ band has a very large moment of inertia, more than twice that of the ground state. The second 2^+ state at 5.8 MeV (expt. 6.0 MeV) and the 3^+ state at 9.6 MeV consist mainly of $K^\pi=2^+$ components, and the 1^+ state at 10.1 MeV and 2_4^+ state at 11.2 MeV is dominantly the $K^\pi=1^+$ (spin-triplet) component.

TABLE V. A list of the basis states we have employed for the GCM calculation of ^{10}Be. Basis states for positive-parity states (upper panel) and for negative-parity states (lower panel).

Configuration	α-α distance (d) (fm)
$\Phi(3/2^-,-3/2^-)$	1.0 2.0 2.5 3.0 3.5 4.0 5.0 6.0
$\Phi(1/2^-,-1/2^-)$	2.0 2.5 3.0 3.5 4.0 5.0 6.0
$\Phi(1/2^+,-1/2^+)$	2.0 3.0 3.5 4.0 4.5 5.0 6.0
π orbit, $S_z=1$ ($\Phi(3/2^-,-1/2^-)$)	2.0 2.5 3.0 3.5 4.0 5.0 6.0
σ orbit, $S_z=1$	2.0 2.5 3.0 3.5 4.0 5.0 6.0

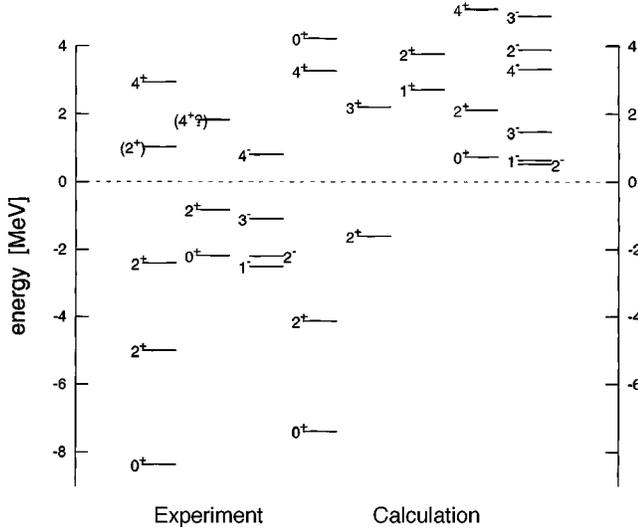| Configuration	α-α distance (d) (fm)
$\Phi(3/2^-,-1/2^+)$	2.0 2.5 3.0 3.5 4.0 4.5 5.0 6.0
$\Phi(3/2^-,1/2^+)$	2.0 2.5 3.0 3.5 4.0 4.5 5.0 6.0
$\Phi(1/2^-,-1/2^+)$	2.0 2.5 3.0 3.5 4.0 4.5 5.0 6.0
$\Phi(1/2^-,1/2^+)$	2.0 2.5 3.0 3.5 4.0 4.5 5.0 6.0

FIG. 5. Calculated and experimental energy levels of ^{10}Be measured from the $\alpha+\alpha+n+n$ threshold. The calculated levels are sorted into five columns. From left to right: states whose dominant component is $K^\pi=0^+$, $K^\pi=2^+$, $K^\pi=1^+$. The fourth column is the second 0^+ band characterized by the σ orbits. The fifth column is the negative-parity band.

The experimentally observed levels are also shown in Fig. 5, in which we can clearly reassign the ground-state rotational band (0_1^+, 0.0 MeV – 2_1^+, 3.4 MeV – 4_1^+, 11.3 MeV). For the second 0^+ band, the 0_2^+ and the 2_3^+ states are observed at 6.3 MeV and 7.5 MeV, respectively, and a candidate for the 4^+ state of this band whose cluster structure is recently discussed [12] is 10.2 MeV. We also obtain a candidate for the $K^\pi=2^+$ band. All of these observed levels have a nice correspondence with the present calculated results.

The calculated ground state is underbound from the $\alpha+\alpha+n+n$ threshold by 1 MeV. To remove this discrepancy, it is necessary to examine the interaction which we use especially for the pairing interaction between the first 0^+ state and the third 0^+ state (this will be discussed later). As for the excited levels, the calculated excitation energy of the second 0^+ band is higher than the observed one by about 2 MeV. This is mainly due to the simple assumption of the σ orbit described as a superposition of four local Gaussians. Since the level has the s wave component, the tail effect of two valence neutrons is expected to be important. We have checked that this underbinding of 2 MeV can be overcome when we represent the tail of the wave function carefully and include the deviation of the σ orbit from the α-α axis within the model space in which the α-α distance (d) is fixed to 4 fm.

The second 0^+ state has a much larger charge radius (2.93 fm; a proton radius of 0.813 fm is used) than the ground state (2.51 fm), which is a signature of the developed α-α structure. As for the configuration of this state, the result based on the shell model supports the contention that valence neutrons occupy not the p orbit, but the sd orbit. In the Cohen-Kurath model [20], where all the configurations in the p shell are taken into account, the excitation energies of

the first and the second 2^+ states almost agree with the experimental values (2^+:3.7 MeV and 2^+:5.4 MeV, experimentally 3.4 MeV and 6.0 MeV, respectively). However, the second 0^+ state is put at 12.35 MeV. This energy is about twice the observed excitation energy of 0_2^+ (6.263 MeV). This result implies that the 0_2^+ state (bandhead of cluster band) cannot be understood within the p shell and the contributions of sd shells are required.

The negative-parity states are also presented. In addition to reproducing the four observed states (1^-, 2^-, 3^-, and 4^-), we predict a second 2^- state and a second 3^- state (the second 4^- state is out of the energy range of this figure). The presence of two states for each J^π is due to a coupling effect between two bands: $K^\pi=1^-$ and $K^\pi=2^-$. In the $K^\pi=1^-$ band, a valence neutron for the π orbit and one for the σ orbit have opposite spin directions ($S_z=0$), and in the $K^\pi=2^-$ band, they have the same spin direction ($S_z=1$). Since the energies of these two bands are close and the coupling between them is strong, there is no clear band structure for the negative-parity states.

Both the calculated and the experimental results reflect this K-mixing effect, and the level spacing between the 1^- state and the 2^- state is very small. If we restrict ourselves to only $K=1$, 1^- is found at -53.0 MeV and 2^- at -52.0 MeV. The level spacing is more than 1 MeV. However, for the 2^- state, the bandhead of the $K=2^-$ band is at -51.6 MeV, and the coupling is very strong. Therefore, when we perform K mixing, the level spacing between these two states becomes much smaller (-53.4 MeV for 1^-, -53.5 MeV for 2^-). Since $K=2$ is a spin triplet, this 2^- state has a strong admixture of the $K=1$ component and the $K=2$ component, just like in the so-called spin vibrational state.

B. Coupling effect between the basis states

In this subsection, the coupling effect between the basis states for the positive-parity states is analyzed. Table VI shows the matrix elements of the Hamiltonian between the basis states with the optimal d value for each configuration.

The matrix element between the ground $\Phi(3/2^-, -3/2^-)$ configuration ($d=3$ fm) and its spin-orbit partner $\Phi(1/2^-, -1/2^-)$ ($d=3$ fm) is equal to -2.8 MeV, which is much larger than the matrix element between the ground-state configuration and the second 0^+ configuration [$\Phi(1/2^+, -1/2^+)$ $d=4$ fm]. Therefore, the pairing between states which consist of the π orbit is stronger than the pairing between the basis states with the π orbit and the state with the σ orbit. After diagonalization of this matrix, the lowest 0^+ state has an energy of -58.7 MeV, which is lower by 0.8 MeV than the value before diagonalization. Here, the third 0^+ state is pushed up to -44.8 MeV (-45.5 MeV before the diagonalization) due to this diagonalization. On the other hand, the second 0^+ has little influence due to pairing. Therefore, the pair coupling affects the level spacing between the $(1/2^-)^2$ configuration and the $(1/2^+)^2$ configuration, and in ^{10}Be it enhances the level inversion.

We can confirm that the third 0^+ state is really excited due to pairing with the ground 0^+ state by artificially changing the matrix element. When the matrix element between

TABLE VI. The matrix element of the Hamiltonian (real, imaginary) between the basis states: $\Phi(3/2^-,-3/2^-)d=3$ fm, $\Phi(1/2^-,-1/2^-)d=3$ fm, and $\Phi(1/2^+,-3/2^+)d=4$ fm. The unit is MeV.

	$\Phi(3/2^-,-3/2^-)$	$\Phi(1/2^-,-1/2^-)$	$\Phi(1/2^+,-3/2^+)$
$\Phi(3/2^-,-3/2^-)d=3$ fm	$(-58.0, 0.0)$	$(-2.8, 0.2)$	$(-0.2, -0.1)$
$\Phi(1/2^-,-1/2^-)d=3$ fm	$(-2.8, -0.2)$	$(-45.5, 0.0)$	$(-0.2, 0.3)$
$\Phi(1/2^+,-1/2^+)d=4$ fm	$(-0.2, 0.1)$	$(-0.2, -0.3)$	$(-46.4, 0.0)$

the ground 0^+ state and the third 0^+ is assumed to be -3.5 MeV, the third 0^+ state is excited to -44.4 MeV ($0^+_1=-59.1$ MeV); if it is 4.0 MeV, the third 0^+ state is excited to -44.1 MeV ($0^+_1=-59.4$ MeV).

C. Large α-α cluster structure in the second 0^+ state

We analyze the enlargement of the α-α distance in the second 0^+ state. The 0^+ energy for each α-α distance is shown in Fig. 6. The solid line in Fig. 6 has a large component of $\Phi(1/2^+,-1/2^+)$, and this energy becomes lower as the α-α distance increases. The energy minimum is found at an α-α distance of 4–5 fm. An enlargement effect of the α-α distance by the $(1/2^+)^2$ configuration in the second 0^+ state of ^{10}Be is clearly shown. Here, the coefficients $\{g\}$ for the Gaussians are also optimized. In spite of this extension of the model space, the configurations introduced above basically keep their structures. The three 0^+ states are well represented by the original three basic configurations. The squared overlap between the ground state and $\Phi(3/2^-,-3/2^-)$ is 0.93 at $d=3$ fm, that between 0^+_2 and $\Phi(1/2^+,-1/2^+)$ is 0.79 at $d=4$ fm, and that between 0^+_3 and $\Phi(1/2^-,-1/2^-)$ is 0.84 at $d=3$ fm. However, as can be seen from the squared overlap of 0.79, the second 0^+ state is not described only by the $\Phi(1/2^+,-1/2^+)$ configuration, but the coupling with the spin-triplet chain orbit (σ orbit) is found to be strong.
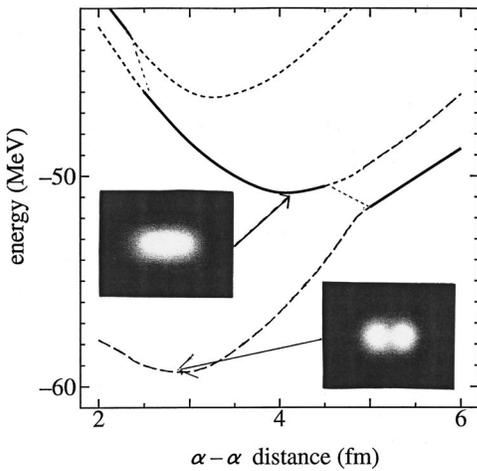

FIG. 6. The α-α (d) dependence of the 0^+ states. There appear three 0^+ states in the low-lying energy region. The solid line shows the state which has an overlap with the $\Phi(1/2^+,-1/2^+)$ configuration dominantly, and the long dashed line shows the $\Phi(3/2^-,-3/2^-)$ configuration.

D. Effect of triplet-odd pairing in the chain orbit

In the traditional MO model, the spin-orbit interaction does not contribute to the $\Phi(1/2^+,-1/2^+)$ configuration. This is because the two valence neutrons spread along the two α clusters, and they cannot rotate around a core nucleus (another reason is that the two valence neutrons occupy the same spatial configurations with opposite spin direction). However, the spin-orbit interaction in the second 0^+ state is taken into account by coupling with the spin-triplet configuration.

Table VII shows the coupling between the $\Phi(1/2^+,-1/2^+)$ ($S_z=0$ in Table VII) and the spin-triplet chain orbits ($S_z=1$ in Table VII) at $d=4$ fm. Both the total energy and the spin-orbit energy are shown. The $\Phi(1/2^+,-1/2^+)$ configuration gives an 0^+ energy of -46.39 MeV, and the spin-orbit interaction does not work for this state. However, it acts strongly for the off-diagonal matrix element between $S_z=0$ and $S_z=1$ (8.11 MeV) which exhausts almost the off-diagonal matrix element. Because of this matrix element, the spin-orbit interaction finally acts attractively in the coupled state. After coupling, the energy of the second 0^+ state becomes -49.53 MeV, about 3 MeV lower than that in the pure $\Phi(1/2^+,-1/2^+)$ state, and the spin-orbit interaction contribution is -4.75 MeV (triplet-odd pairing in the chain orbits). This large effect is never negligible for a description of the second 0^+ state. The spin-orbit interaction plays its role to enhance the level inversion of the two 0^+ states $(1/2^+)^2$ and $(1/2^-)^2$.

Recently, a theoretical analysis based on the microscopic $\alpha+\alpha+n+n$ model using the stochastic variational method (SVM) has been performed [21]. The calculation also shows the contribution of the $S=1$ component in the second 0^+ state. The component of $S=1$ is 23.1% in the second 0^+ state; this value almost agrees with our result discussed in the last part of the previous subsection.

E. Electromagnetic transition

A physical quantity signaling a pronounced α-α structure in the second 0^+ state is $B(E2)$ [their values are listed in

TABLE VII. The coupling effect between the $S_z=0$ chain orbits (σ orbits) and the $S_z=1$ chain orbits for the basis states of the second 0^+ state. The energies and their spin-orbit components (written as ls) are shown.

	$S_z=0$	$S_z=1$	Off-diagonal	Coupled
Energy (MeV)	-46.39	-28.59	-8.11	-49.53
ls (MeV)	0.00	5.47	-8.11	-4.75

TABLE VIII. (A) $B(E2)$ of ^{10}Be $2^+ \rightarrow 0^+$; the unit is e^2 fm^4. The value in parentheses is an experimental datum. (B) $B(E1)$ of ^{10}Be $1^- \rightarrow 0^+$; the unit is e^2 fm^2.

| | (A) | |
	0_1^+	0_2^+
2_1^+	11.26 (10.04±1.2)	0.23 (0.65±0.40)
2_2^+	0.44	0.00
2_3^+	0.19	35.56

| | (B) | |
	0_1^+	0_2^+
1^-	2.36×10^{-3}	2.06×10^{-3} $(4.22 \pm 1.51 \times 10^{-3})$

Table VIII together with those of $B(E1)$]. $B(E2 2_3^+ \rightarrow 0_2^+)$ is predicted to be 35.72 e^2 fm^4, which is about 3 times the yrast one [$B(E2 2_1^+ \rightarrow 0_1^+) = 11.46$ e^2 fm^4, experimentally 10.04 ± 1.2 e^2 fm^4]. If this huge transition is measured, it would provide very strong evidence for a large α-α structure. Unfortunately, the neutron threshold opens at 6.81 MeV between 0_2^+ (6.18 MeV) and 2_3^+ (7.54 MeV), which makes the measurement difficult. The width of the neutron emission is 6.3 ± 0.8 keV [22].

Recently, a candidate for this cluster band structure has been observed in ^{10}Be. Fragments of α and ^{6}He from a state at 10.2 MeV have been observed and the state fits into the $J(J+1)$ rule along with the second 0^+ state (6.26 MeV [22]) and the third 2^+ state (7.54 MeV). This is thus believed to be 4^+, and belongs to a cluster rotation band whose bandhead is the second 0^+ state.

VI. DISCUSSION OF THE BINDING MECHANISM

In this section, the binding mechanisms in the ground 0^+ state and in the second 0^+ state are discussed. These discussions are related to the physical meaning of the description based on the MO model.

A. Binding mechanism for the ground state

In this subsection, the binding mechanism of ^{10}Be is analyzed, and each contribution of the Hamiltonian to the binding energy is clarified. The ground state of ^{10}Be is bound by 8.38 MeV from the $\alpha + \alpha + n + n$ threshold. This is a rather large binding energy, since ^{8}Be does not have a bound state of α-α and ^{9}Be is bound from the $\alpha + \alpha + n$ threshold by only 1.67 MeV. Thus, the binding of 8.38 MeV from the four-body threshold in ^{10}Be is larger than twice the neutron binding energy in ^{9}Be by 5 MeV. This is a problem which we are going to discuss.

As for the potential-energy term of the Hamiltonian, the contribution of this term is far from accounting for the remaining 5 MeV. In the previous subsection, we showed that the pairing interaction between the ring-orbit configurations pushes down the ground 0^+ state. This effect increases the binding energy only by 1 MeV, which is also not enough to solve the problem.

Therefore, we now examine the contribution of the kinetic-energy term and show what the difference is between ^{10}Be and ^{8}Be. The relative kinetic energy between the two clusters in ^{10}Be is compared with that of ^{8}Be. ^{10}Be consists of two configurations (^{6}He$+\alpha$ and ^{5}He$+^5$He). When the α-α distance (d) is equal to 3 fm, the relative kinetic energy between α and ^{6}He [$T(^{10}$Be$) - T(^6$He$) - T(\alpha)$; T is the expectation value of the kinetic energy] is 18.42 MeV. The kinetic energy between ^{5}He and ^{5}He [$T(^{10}$Be$) - T(^5$He$) - T(^5$He$)$] is 18.77 MeV. On the other hand, in ^{8}Be, the relative kinetic energy between the two α clusters [$T(^8$Be$) - 2 \times T(\alpha)$] is 22.63 MeV. Therefore, there is a decrease in the kinetic energy by 4 MeV from ^{8}Be to ^{10}Be in the relative motion between the two clusters.

This is due to a drastic change of the reduced mass in ^{10}Be compared with ^{8}Be and ^{9}Be, which is intuitively understood as follows.[1] In ^{8}Be, since the two α clusters are localized at a distance, the reduced mass number corresponding to the relative motion between the two α clusters is

$$\frac{m_1 \times m_2}{m_+ m_2} = \frac{4 \times 4}{4+4} = 2.$$

However, in ^{10}Be, the ^{6}He$+\alpha$ component has a reduced mass number of

$$\frac{m_1 \times m_2}{m_+ m_2} = \frac{6 \times 4}{6+4} = 2.4$$

and the ^{5}He$+^5$He component has a reduced mass number of

$$\frac{m_1 \times m_2}{m_+ m_2} = \frac{5 \times 5}{5+5} = 2.5,$$

and these values are about (20–25)% larger than the value for ^{8}Be. If the energy curvature with respect to the distance between the two clusters (or optimal distance between them) is almost the same, the relative kinetic energy depends only on the inverse of this reduced mass. In such a situation, the reduction of the kinetic energy from ^{8}Be to ^{10}Be is estimated to be around 20% (about 4 MeV). Therefore, the large binding energy of ^{10}Be (8.38 MeV from the four-body threshold) can be fully explained when we take into account all of these contributions.

Next, we show the mechanism which stabilizes the clustering feature of the ground state in spite of the substantial binding energy from the four-body threshold. This is related to the physical meaning of the MO. In a calculation based on AMD [16], the ground state has been obtained to be a ^{6}He $+ \alpha$-like configuration where each valence neutron has been expressed by a single Gaussian. On the other hand, in the MO model, the valence neutrons rotate around both α clusters. Then the amplitudes of the ^{6}He$+\alpha$ and ^{5}He$+^5$He

----

[1]This idea of the reduced mass number comes from a discussion with Professor K. Ikeda.

model spaces are equally mixed. We show the coupling effect of ^{5}He+^{5}He on ^{6}He+α for the $\Phi(3/2^-, -3/2^-)$ configuration. Here, the ^{6}He+α and ^{5}He+^{5}He configurations only mean whether two valence neutrons rotate around the same α cluster or around different α clusters. Therefore, of course, the ^{6}He+α model space is not the same as the free ^{6}He, with a halo structure and an α cluster. The ^{6}He+α [$\Phi({}^6$He+$\alpha)$] model space consists of terms where two valence neutrons occupy the AO around the same α cluster (at $+a$ or $-a$ on the z axis),

$$\Phi({}^6\text{He}+\alpha) = \mathcal{A}[\phi_1^{(\alpha)}\phi_2^{(\alpha)}(p_x+ip_y)_{+a}|n\uparrow\rangle$$

$$\times (p_x-ip_y)_{+a}|n\downarrow\rangle] \tag{29}$$

$$+ \mathcal{A}[\phi_1^{(\alpha)}\phi_2^{(\alpha)}(p_x+ip_y)_{-a}|n\uparrow\rangle$$

$$\times (p_x-ip_y)_{-a}|n\downarrow\rangle], \tag{30}$$

while the ^{5}He+^{5}He model space [$\Phi({}^5$He+^{5}He)] consists of terms where they occupy the AO around different α clusters (at $+a$ and $-a$ on the z axis),

$$\Phi({}^5\text{He}+{}^5\text{He}) = \mathcal{A}[\phi_1^{(\alpha)}\phi_2^{(\alpha)}(p_x+ip_y)_{+a}|n\uparrow\rangle$$

$$\times (p_x-ip_y)_{-a}|n\downarrow\rangle] \tag{31}$$

$$+ \mathcal{A}[\phi_1^{(\alpha)}\phi_2^{(\alpha)}(p_x+ip_y)_{-a}|n\uparrow\rangle$$

$$\times (p_x-ip_y)_{+a}|n\downarrow\rangle]. \tag{32}$$

Parameters a and b are the same as in the upper panel of Table II.

Figure 7 is the 0^+ energy curves obtained by changing the mixing weight of two model spaces. The left-hand-side limit has only ^{6}He+α, and the right-hand-side limit ^{5}He+^{5}He. When the α-α distance is small, the ^{6}He+α and ^{5}He+^{5}He spaces have a large overlap; thus, even if the ^{5}He+^{5}He amplitude increases, the energy curve is flat. However, when the α-α distance is around 3 fm (the optimal distance of ^{10}Be), the coupling effect due to the exchange of a neutron from one cluster to another cluster is about 1.3 MeV. There, the ^{6}He+α and the ^{5}He+^{5}He configurations have equal amplitudes.

In Table IX, we give the calculated total, kinetic, and potential energies at $d=3$ fm for three cases: the ^{6}He+α model space, the ^{5}He+^{5}He model space, and mixed model space. The total energy gain from the ^{6}He+α model space (-56.87 MeV) to the mixed model space (-58.15 MeV) is about 1.3 MeV. However, if we consider only the potential energy, its value in the mixed space (-206.71 MeV) is not lower than in the ^{6}He+α space (-206.82 MeV). Then, the binding-energy gain must come from the kinetic-energy reduction. This mixing of these two configurations may be said to be due to the exchange of one neutron from one α cluster to another α cluster produced by the kinetic-energy operator, and that extends the region available for the valence neutrons and decreases the kinetic energy. The realization of the mixed state is the physical meaning of the ring orbit (π orbit) in the MO model. If the α-α distance is smaller than $d=3$ fm, the space available for the valence neutrons is not
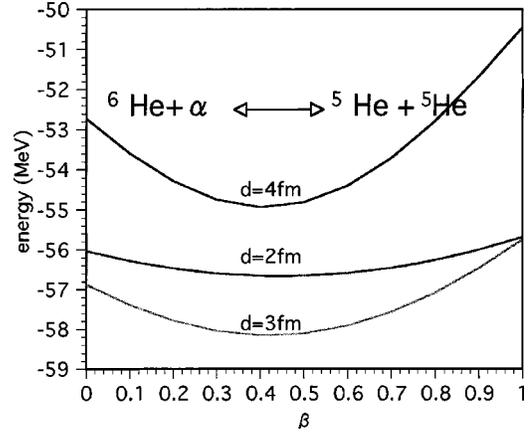

FIG. 7. The 0^+ energy curve of $(1-\beta)\Phi({}^6$He+$\alpha)+\beta\Phi({}^5$He+^{5}He) obtained by changing β. The left-hand-side limit is ^{6}He+α and the right-hand-side limit is ^{5}He+^{5}He. The numbers in the figure are the values of the α-α distance (d).

enough and the coupling effect is small. On the other hand, if the α-α distance is too large, the valence neutrons are localized around one of the α clusters; then the coupling effect is also small. The coupling effect between the ^{6}He+α and the ^{5}He+^{5}He model spaces becomes maximal around $d=3$ -4 fm. Therefore, in spite of the sufficient binding energy (8.38 MeV from the $\alpha+\alpha+n+n$ threshold), the ground state of ^{10}Be keeps the cluster structure to provide an available region for the valence neutrons. It is clearly shown in Fig. 8 that the optimal α-α distance for the mixed model space is larger than for either the ^{6}He+α or the ^{5}He+^{5}He spaces by 0.3 fm.

We can state that this coupling between the two configurations plays a decisive role for the stabilization of the α-α structure surrounded by two neutrons in ^{10}Be. Finally, we should note that this persistence of the α-α clustering structure surrounded by two neutrons accounts for the above-mentioned large reduction of the kinetic energy between the two clusters.

B. Binding mechanism for the second 0^+ state

In this subsection, the binding mechanism of the second 0^+ state, which is dominated by the $(1/2^+)^2$ configuration, is analyzed, and this is related to the physical meaning of the σ orbit. According to a description based on the MO model, the neutrons which occupy the σ orbit rotate around both α

TABLE IX. The coupling effect between the ^{6}He+α model space and the ^{5}He+^{5}He model space for the basis states of the first 0^+ state. Total, kinetic, and potential energies for both the ^{6}He+α and the ^{5}He+^{5}He model spaces are shown at the α-α distance of 3 fm.

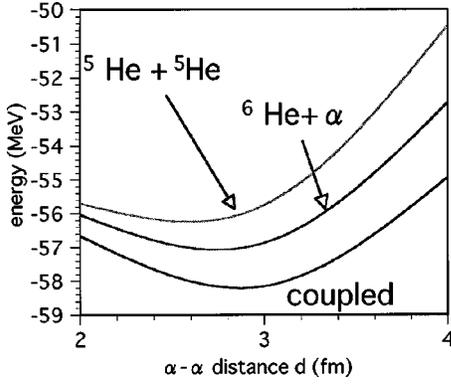|	^{6}He+α	^{5}He+^{5}He	Mixing
Total (MeV)	-56.87	-55.75	-58.15
Kinetic (MeV)	149.94	149.74	148.55
Potential (MeV)	-206.82	-205.49	-206.71

FIG. 8. The 0^+ energy curve for the $\Phi(3/2^-, -3/2^-)$ configuration. The dotted line shows the $^6\text{He}+\alpha$ model space and the dashed line corresponds to the $^5\text{He}+{}^5\text{He}$ model space. The horizontal axis is the α-α distance (d).
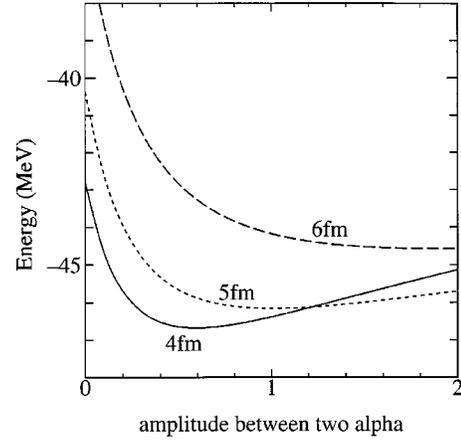

FIG. 9. The 0^+ energy curve of the $\Phi(1/2^+, -1/2^+)$ configuration obtained by changing the distribution of the valence neutrons between the two α clusters. The value $\delta=1$ corresponds to the original amplitude of the MO model. The α-α distances are displayed in this figure.

clusters symmetrically, and spread widely along the α-α axis. This σ orbit plays a role to enhance the α-α distance; however, in the MO model, the neutrons have their density between the α clusters, and this component increases the potential energy. As can be seen in Fig. 1(b), the σ orbit is expressed by four Gaussians on the α-α axis:

$$\phi_{ci} = \{(\vec{p})_{d/2} - (\vec{p})_{-d/2}\}|n\uparrow\rangle$$
$$= \{G_{(d/2\vec{e}_z+\vec{b}} - G_{(d/2)\vec{e}_z-\vec{b}}$$
$$- G_{-(d/2)\vec{e}_z+\vec{b}} + G_{-(d/2)\vec{e}_z-\vec{b}}\}|n\uparrow\rangle. \quad (33)$$

Here, $d/2$ and $-d/2$ are the positions of the two α clusters, and for example, $G_{(d/2)\vec{e}_z+\vec{b}}$ is a Gaussian whose center is at $(d/2)\vec{e}_z+\vec{b}$. In the MO model, a neutron amplitude along the z axis in between the two α clusters is explicitly described by the second and third Gaussians in Eq. (33). By changing the amplitude of the two Gaussians along the z axis in between α-α, we obtain the 0^+ energy curve shown in Fig. 9. Parameter b_z is fixed at 2.0 fm. The abscissa corresponds to δ, the amplitude in between the two α clusters.

$$\phi_{ci} = \{(\vec{p})_{d/2} - (\vec{p})_{-d/2}\}|n\uparrow\rangle$$
$$= \{G_{(d/2)\vec{e}_z+\vec{b}} - \delta(G_{(d/2)\vec{e}_z-\vec{b}}$$
$$+ G_{-(d/2)\vec{e}_z+\vec{b}}) + G_{-(d/2)\vec{e}_z-\vec{b}}\}|n\uparrow\rangle. \quad (34)$$

The value $\delta=1$ is around the original amplitude of the two Gaussians, and at $d=4$ fm [the optimal distance for $\Phi(1/2^+, -1/2^+)$], the energy minimum corresponds to almost 1. If amplitude δ vanishes between the clusters, the 0^+ energy becomes higher by several MeV. As the α-α distance increases, this amplitude becomes more important, since it supplies potential energy to the two distant α clusters. These results show that the σ orbit allows the α-α distance to spread, thus weakly connecting the clusters.

VII. CONCLUSION

We have applied the $\alpha+\alpha+n+n$ model to ^{10}Be, where the orbits for the valence neutrons have been introduced based on the molecular orbit (MO) model. All of the low-lying positive and negative-parity states of ^{10}Be have been clearly described by combinations of three basic orbits for the valence neutrons around the two α clusters. These orbits originate from the low-lying $3/2^-$, $1/2^+$, and $1/2^-$ states in ^9Be. We have studied the behavior of the α-α core for each configuration of the valence neutrons.

In the present model, the spatially extended motion of valence neutrons around the α clusters is described by linear combinations of Gaussians, and the centers of the Gauusians are variationally determined. Because of this extension of the model space, it is possible to use the strength of the spin-orbit interaction, which is determined by an analysis of the α-n scattering. The strength has been artificially weakened to less than half in the traditional MO models.

In ^{10}Be, the ground state and the third 0^+ state are characterized by the π orbit of the valence neutrons. A π orbit has only one node perpendicular to the α-α axis, and the spin-orbit interaction splits the π orbit into $K^\pi=3/2^-$ and $1/2^-$. The 0^+ ground state dominantly has the $(3/2^-)^2$ configuration, and the third 0^+ state has the $(1/2^-)^2$ configuration.

The ground state is bound rather strongly (8.38 MeV) from the $\alpha+\alpha+n+n$ threshold, and the binding mechanism has been discussed. The pairing effect between the $(3/2^-)^2$ state and the $(1/2^-)^2$ state gives rise to an increase of the binding energy by about 1 MeV; however, the most important effect is the reduction of the relative kinetic energy between the two clusters in comparison with ^8Be. If we take into account these effects, the mechanism of this large binding can be fully understood. In spite of this large binding, the α-α clustering in the ground state persists. This is due to a coupling effect between the $^6\text{He}+\alpha$ configuration and the $^5\text{He}+{}^5\text{He}$ configuration, which provides a smooth potential

for the valence neutrons and reduces the kinetic energy of two valence neutrons by 1.3 MeV.

The second 0^+ state has a large α-α distance, which is characterized by the σ orbit. The two valence neutrons stay along the α-α axis (the $1/2^+$ orbit) and reduce the kinetic energy by enhancing the α-α distance. The two α clusters are weakly bound due to an interaction with the valence neutron spreading widely along the α clusters. A large $E2$ transition probability between states which belong to a rotational band (0_2^+, 2_3^+, 4_2^+) is a signature for the presence of such states.

The binding mechanism of the second 0^+ state other than the enlargement of the α-α distance has also been discussed. The contribution of the spin-orbit interaction due to the coupling between the $S_z = 0$ and the $S_z = 1$ configurations is important for the state. The mediation effect of two valence neutrons between two α clusters is also important for a quantitative description of the state. The calculated excitation energy of the second 0^+ state is slightly higher (~ 2 MeV) than the experimental one. Therefore, we will describe it more correctly by reproducing the tail of the valence neutrons in future work.

We have theoretically pointed out that the level inversion between $1/2^-$ and $1/2^+$ in ^{9}Be also holds in ^{10}Be. The $1/2^+$ state has been observed to be lower than the $1/2^-$ state also in ^{11}Be. This result suggests a possibility that the component of the $(1/2^+)^2$ configuration mixes in the ground state of ^{12}Be. This means a breaking of the closed p-shell configuration in $N = 8$; the present analysis gives a perspective for a systematic study of Be isotopes beyond $N = 8$. As future work, we are going to perform a systematic analysis based on the present result up to the drip-line nucleus ^{14}Be.

[1] I. Tanihata, T. Kobayashi, O. Yamakawa, S. Shimoura, K. Ekuni, K. Sugimoto, N. Takahashi, T. Shimoda, and H. Sato, Phys. Lett. B **206**, 592 (1988).

[2] *Proceedings of the International Symposium on Physics of Unstable Nuclei*, Niigata, 1995 [Nucl. Phys. **A588**, 1 (1995)]; *Proceedings of the Fourth International Conference on Radioactive Nuclear Beam*, Omiya, 1996 [Nucl. Phys. **A616**, 1 (1997)].

[3] I. Tanihata, J. Phys. G **22**, 157 (1996).

[4] T. Suzuki and T. Otsuka, Phys. Rev. C **56**, 847 (1997).

[5] D. Brink, in *Proceedings of the International School of Physics ''Enrico Fermi,''* Course 36, Varenna, 1965, edited by C. Bloch (Academic, New York, 1966), p. 247.

[6] Y. Fujiwara, H. Horiuchi, K. Ikeda, M. Kamimura, K. Katō, Y. Suzuki, and E. Uegaki, Suppl. Prog. Theor. Phys. **68**, 60 (1980).

[7] S. Okabe, Y. Abe, and H. Tanaka, Prog. Theor. Phys. **57**, 866 (1977); S. Okabe and Y. Abe, *ibid.* **59**, 315 (1978).

[8] S. Okabe and Y. Abe, Prog. Theor. Phys. **61**, 1049 (1979).

[9] H. Furutani, H. Kanada, T. Kaneko, S. Nagata, H. Nishioka, S. Okabe, S. Saito, T. Sakuda, and M. Seya, Suppl. Prog. Theor. Phys. **68**, 193 (1980).

[10] M. Seya, M. Kohno, and S. Nagata, Prog. Theor. Phys. **65**, 204 (1981).

[11] Y. Abe, J. Hiura, and H. Tanaka, Prog. Theor. Phys. **49**, 800 (1973).

[12] N. Soić *et al.*, Europhys. Lett. **34**, 7 (1996).

[13] A.B. Volkov, Nucl. Phys. **74**, 33 (1965).

[14] N. Yamaguchi, T. Kasahara, S. Nagata, and Y. Akaishi, Prog. Theor. Phys. **62**, 1018 (1979).

[15] Y. Kanada-En'yo and H. Horiuchi, Prog. Theor. Phys. **93**, 115 (1995).

[16] Y. Kanada-En'yo, H. Horiuchi, and A. Ono, Phys. Rev. C **52**, 628 (1995).

[17] Y. Kanada-En'yo and H. Horiuchi, Phys. Rev. C **52**, 647 (1995).

[18] A. Doté, H. Horiuchi, and Y. Kanada-En'yo, Phys. Rev. C **56**, 1844 (1997).

[19] A. Ono, H. Horiuchi, T. Maruyama, and A. Ohnishi, Prog. Theor. Phys. **87**, 1185 (1992); Phys. Rev. Lett. **68**, 2898 (1992).

[20] S. Cohen and D. Kurath, Nucl. Phys. **73**, 1 (1965).

[21] Y. Ogawa, K. Arai, Y. Suzuki, and K. Varga, Report No. RIKEN-AF-NP-291, 1998.

[22] F. Ajzenberg-Selove, Nucl. Phys. **A490**, 1 (1988).